Original Article

Damage localization with fiber Bragg grating Lamb wave sensing through adaptive phased array imaging

Zhenhua Tian, Lingyu Yu, Xiaoyi Sun and Bin Lin

Abstract

Fiber Bragg gratings are known being immune to electromagnetic interference and emerging as Lamb wave sensors for structural health monitoring of plate-like structures. However, their application for damage localization in large areas has been limited by their direction-dependent sensor factor. This article addresses such a challenge and presents a robust damage localization method for fiber Bragg grating Lamb wave sensing through the implementation of adaptive phased array algorithms. A compact linear fiber Bragg grating phased array is configured by uniformly distributing the fiber Bragg grating sensors along a straight line and axially in parallel to each other. The Lamb wave imaging is then performed by phased array algorithms without weighting factors (conventional delay-and-sum) and with adaptive weighting factors (minimum variance). The properties of both imaging algorithms, as well as the effects of fiber Bragg grating's direction-dependent sensor factor, are characterized, analyzed, and compared in details. The results show that this compact fiber Bragg grating array can precisely locate damage in plates, while the comparisons show that the minimum variance method has a better imaging resolution than that of the delay-and-sum method and is barely affected by fiber Bragg grating's direction-dependent sensor factor. Laboratory tests are also performed with a four–fiber Bragg grating array to detect simulated defects at different directions. Both delay-and-sum and minimum variance methods can successfully locate defects at different positions, and their results are consistent with analytical predictions.

Introduction

Structural health monitoring (SHM) is critical to maintain the safety of structural components and provide input data for failure and remaining life predictions in various fields, such as aerospace, civil and nuclear engineering.[1,2] Among various methods, Lamb waves (plate guided waves) have shown great potentials for health monitoring and in situ damage detection in large plate-like structures, due to their sensitivity to small damage and capability of traveling relatively long distances compared to traditional bulk waves.[3,4] Advances in Lamb wave–based SHM technologies, such as sparse arrays and phased arrays, have demonstrated their effectiveness and efficiency for damage detection in large plate-like structures.[5–8]

Recently, fiber Bragg gratings (FBGs) are emerging as Lamb wave sensors for SHM. FBG sensors have the advantage of immune to electromagnetic interference, compared to the commonly used piezoelectric transducers

(PZT).[9,10] Moreover, FBG sensors are small, lightweight, and capable of working in unfavorable environments such as wet, underwater, and high temperatures.[11–13] Furthermore, FBG sensors offer the possibility of multiplexing several FBGs of different grating periods on the same optical fiber and interrogating them individually.[14,15] With these advantages, FBG sensors have been adopted for Lamb wave sensing based on the full-width-half-maximum (FWHM) principle for damage detection and source localization in metallic and composite plates.[9,12,16–22] For example, Takeda et al.[13] developed small-diameter optical fibers with FBG sensors, which can be embedded in

Department of Mechanical Engineering, University of South Carolina, Columbia, SC, USA

Corresponding author:
Lingyu Yu, Department of Mechanical Engineering, University of South Carolina, 300 Main Street, Columbia, SC 29208, USA.
Email: yu3@cec.sc.edu

a lamina, for sensing Lamb waves and detecting damage in composite structures. In their method, the Lamb wave sensing was based on the wavelength shift detected by a high-speed optical wavelength interrogation system. Later, the small-diameter FBG sensor was embedded in the adhesive layer between a honeycomb core and a skin plate for debonding detection.[23] Tsuda et al.[17] developed a hybrid system using PZT to generate and FBG sensors to measure Lamb waves for impact damage detection in composite plates. Lam et al.[12] used a PZT and an embedded FBG in composite plates in the pitch-catch setup for delamination evaluation. However, it has been found that FBG sensors have direction-dependent sensor factor and exhibit strongest sensing along the fiber direction. Hence, judiciously configuring a group of FBG sensors is essential for using these direction-dependent sensors for locating damage which might present in any directions in the structure. For this purpose, Kirkby et al.[19] demonstrated impact localization in composite plates using a sparse network of FBG sensors and an iterative localization algorithm based on optimization scheme. Wu et al.[18] employed a distributed hybrid PZT-FBG sensor network for debond detection in composite laminates using damage index defined by scattering energy at defects. However, the direction-dependent sensing of FBG is not discussed by either. Betz et al.[16] carefully studied the direction dependence of FBG Lamb wave sensing and concluded the FBG sensor factor. An FBG rosette method for damage localization was therefore developed with the sensor factor in consideration. However, the localization requires two rosettes which seem to require a large space to accommodate.

The Lamb wave phased array imaging is very attractive for damage localization in large plate-like structures, since it employs a small number of sensors placed close to each other in a compact format and enables a quick inspection of large areas through phase/time delays in a way analogous to radar.[24] Additional advantages of Lamb wave phased arrays include reinforced wave energy in the beam, efficient and flexible control of the beam direction, improved signal-to-noise-ratio, and large area inspection through a small sensing area.[3] With these features, intensive studies have been conducted on Lamb wave phased arrays for damage detection in large plate-like structures.[7,24–37] The general beamforming algorithms for isotropic materials have been developed[24,25] in various configurations such as one-dimensional (1D) linear arrays[28,38] and two-dimensional (2D) planar arrays.[7,24,29] The phased array approach has been implemented with different types of sensors such as PZT wafers and electromagnetic acoustic transducers (EMAT),[7,24,25,39,40] which are omni-directional transducers.

Hence, our study focuses on developing an innovative damage localization methodology for the direction-dependent FBG Lamb wave sensing through the compact phased array configuration and adaptive phased array imaging, which has not been reported in literatures to the best knowledge of the authors. Linear FBG phased arrays are configured by linearly and uniformly distributing FBG sensors that are axially in parallel. The FBG array imaging is then performed using two methods, the nonadaptive delay-and-sum (DAS) and adaptive minimum variance (MV) methods. The performances of DAS and MV methods are analytically characterized and compared in details. Laboratory experiments are performed with a four-FBG array to detect defects at different directions. Both DAS and MV methods successfully detect the damage location with errors less than 5 mm. It is found that the adaptive MV method is less affected by directional sensitivity of FBG sensors and generates higher resolution images compared to those of the DAS method.

The remainder of this article is organized as follows: section "Lamb wave sensing with FBG sensors" briefly presents the experimental setup of FBG Lamb wave sensing and the investigation of the direction-dependent sensor factor. Section "FBG phased array imaging" develops FBG phased array imaging algorithms and validates the imaging analytically, as well as compares the nonadaptive and adaptive algorithms. Section "Damage detection with FBG phased arrays" presents laboratory experiments of using a four-FBG phased array to detect defects at different directions. Section "Conclusion" concludes the article with findings, discussion, and suggestions for future work.

Lamb wave sensing with FBG sensors

In this section, an experiment is performed to investigate the direction-dependent sensor factor of FBG in order to develop appropriate imaging algorithms for phased arrays made of FBG.

FBG Lamb wave sensing setup

Figure 1(a) and (b) presents a schematic and a photo of the experimental setup for Lamb wave sensing with the FBG. The Cartesian coordinate system is pre-defined with its origin O set at the center of a test plate. A T3003 aluminum plate (610 × 610 × 1, unit: mm) is used in the sensing directionality study. A 10-mm FBG sensor manufactured by AtGrating Technologies is bonded on the plate. The center of the FBG is at the origin O, and the fiber direction (longitudinal) is along the y axis as illustrated. The bonded FBG sensor can measure Lamb waves in the plate, based on the FWHM principle.[10,20,21] Figure 1(c) provides the reflection spectrum of the FBG sensor, which shows a narrow reflection band with a center wavelength of 1549.87 nm and
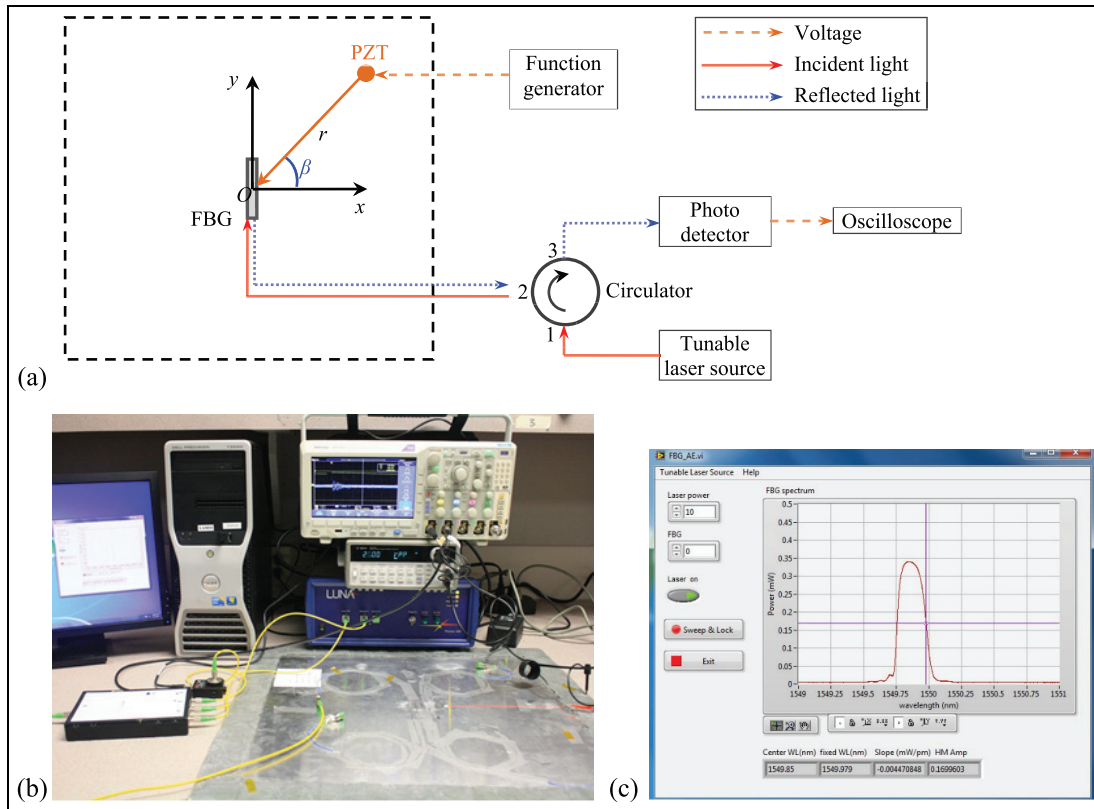
Figure 1. Experimental setup of Lamb wave sensing using an FBG sensor: (a) a schematic of the overall setup, (b) a photo of the test setup, and (c) reflection spectrum of the FBG. Here, the cursor cross on the trailing edge represents the FWHM point. In this study, the laser wavelength is locked at the FWHM point.

a bandwidth of 0.3 nm. A tunable laser source (LUNA Phoenix TLS1400) is used to generate laser light with the wavelength λ_{FWHM} = 1549.98 nm at the FWHM point on the trailing edge based on the initial wavelength sweep and calculation by the software.[22] After passing a circulator (AFW Technologies Pty Ltd, #CIR-3-15L-1-2), the laser light transmits to the FBG. The reflected light from the FBG is then sent to a photodetector (Thorlabs PDA10CF) through the circulator. The photodetector converts light intensity to voltage, which is measured by an oscilloscope (Tektronix TDS5034B). To further improve the signal-to-noise ratio (SNR), the measurement is averaged in the oscilloscope. More details of the FBG Lamb wave sensing can be found in our previous publication.[22]

To excite Lamb wave, PZT wafers (APC 851, 7 mm diameter and 0.2 mm thickness) are bonded on the plate and connected to a function generator (Agilent 33522B). The excitation being used is three-count tone bursts at 270 kHz with 10 V. The PZT wafers are arranged at r = 200 mm away from the origin O at an angle β with respect to the x axis (as illustrated in Figure 1). Nine cases (β = 0°, 10°, 20°, 30°, 45°, 60°, 70°, 80°, and 90°) are studied, respectively.

FBG direction-dependent sensing and sensor factor

Figure 2(a) plots a waveform received by the FBG sensor, when β = 60° after being averaged 100 times in the oscilloscope with SNR[3] of 24. The signal is then further denoised by a band pass filter (100–450 kHz) through post-processing in MATLAB to further reduce the floor noise, as shown in Figure 2(b). The waveform manifests at the excitation frequency 270 kHz, and the wave has a strong S_0 mode (verified by exhibited group velocity at 5.4 mm/μs). Note that there is no A_0 mode in the received waveform. One reason is that the PZT wafer generates a strong S_0 mode with the A_0 mode almost zero at 270 kHz in the subject plate, due to the mode tuning effect of the PZT wafer.[3] The other possible reason is that the FBG sensor is relatively insensitive to the out-of-plane strain (dominated in the A_0 mode) compared to the in-plane strain (dominated in the S_0 mode).[16] Hence in the subsequent sections, S_0 mode will be investigated and used for imaging.

Figure 2(c) plots the normalized amplitudes of S_0 mode from PZT wafers at all the angles. The normalization is performed by dividing the amplitudes for different directions to the amplitude for 90°. The normalized
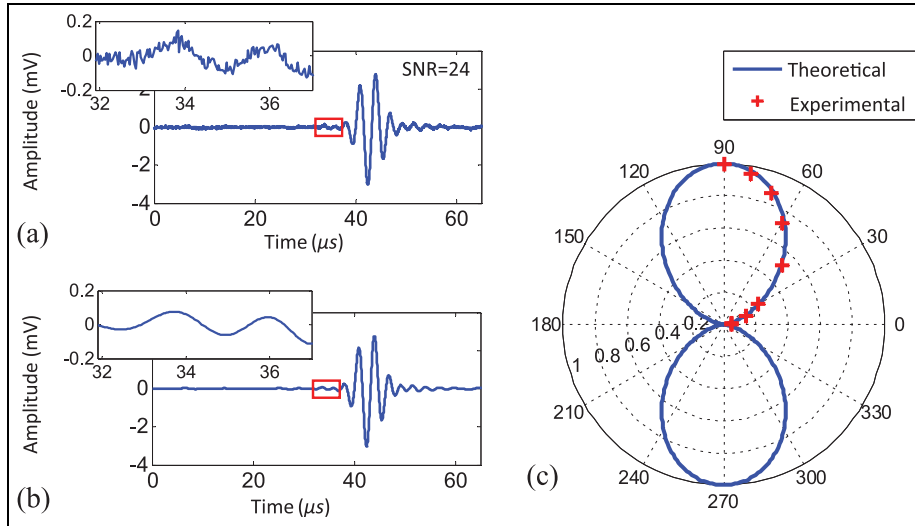
Figure 2. Experimental results. (a) A signal acquired by the FBG when β = 60°. The signal is averaged 100 times and the SNR is 24. (b) The acquired signal is further denoised by a 100–450 kHz band pass filter through the post-processing in MATLAB. (c) The normalized experimental amplitudes of FBG agree well with the theoretical direction-dependent sensor factor for different angles. The normalized is performed by dividing the amplitudes for different angles to the amplitude for 90°.
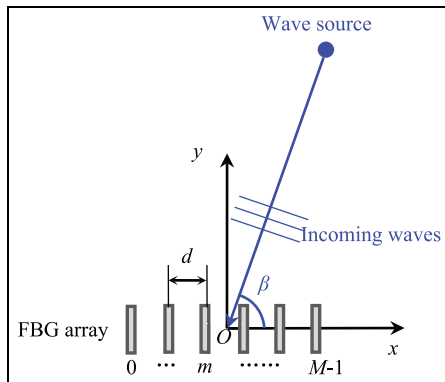
Figure 3. Sensing schematic of a linear FBG array of *M* elements for detecting a wave source.

experimental results agree well with the analytical prediction (solid line) acquired by the following equation[16]

$$A(\beta) = \sin^2(\beta) \qquad (1)$$

where $A(\beta)$ represents the direction-dependent sensor factor of the FBG with respect to angle β. The plots show that at $\beta = 90°$ when the incident wave is along the FBG fiber direction, the sensor factor has the maximum, that is, FBG has the maximum sensitivity to detect the incoming Lamb waves. However, at $\beta = 0°$ when the incident wave is perpendicular to the FBG fiber direction, the sensor factor has the minimum, that is, FBG has the minimum or negligible sensitivity to detect incoming Lamb waves. This direction-dependent

sensor factor makes FBG essentially different from the omni-directional sensors such as PZT wafers[24] used in conventional phased arrays and should be considered in their subsequent FBG phased array imaging.

FBG phased array imaging

To address the challenges caused by the directional sensing of FBG sensors, the FBG phased array imaging was developed using linearly distributed FBG sensors which are parallel to each other. Two imaging algorithms consider the FBG direction-dependent sensor factor and include the nonadaptive conventional DAS and the adaptive MV methods. The imaging algorithms are analytically characterized and compared. The effects of FBG's sensor factor on imaging are also investigated.

FBG array configuration

Figure 3 shows a schematic of a linear FBG phased array made of a total of *M* FBG sensors with the array center designated as the origin *O* of the Cartesian coordinates. The FBG sensors are parallel to each other with fiber direction being aligned with the *y* axis and a uniform spacing *d*. The coordinates of the *m*th ($m = 0$, $1,..., M - 1$) sensor indicated by its center therefore can be given as follows

$$\mathbf{p}_m = \left(\left(m - \frac{M-1}{2}\right)d, 0\right) \qquad (2)$$

Now assume there is a wave source (e.g. actuator, scatterer) at location **x** which is assumed being far away from the FBG array[41] and generating a single Lamb mode coming toward the array with an angle β with respect to the x axis. Considering the direction-dependent sensor factor $A(\beta)$ of the FBG (described in equation (1)), the actual received signal $v_m^\beta(t)$ by the mth FBG can be expressed as follows

$$v_m^\beta(t) = A(\beta)v_m(t) \tag{3}$$

where $v_m(t)$ is the actual wave arriving at location $\mathbf{p}_m$ without FBG sensing. The frequency spectrum $V_m^\beta(\omega)$ of the FBG signal can be obtained through Fourier transform, that is

$$V_m^\beta(\omega) = \mathcal{F}[A(\beta)v_m(t)] = A(\beta)V_m(\omega) \tag{4}$$

where

$$V_m(\omega) = \mathcal{F}[v_m(t)] = \int_{-\infty}^{\infty} v_m(t)e^{-j\omega t}dt \tag{5}$$

Here, $\mathcal{F}[\ ]$ denotes the Fourier transform.

Phased array imaging algorithms

Nonadaptive DAS method. The traditional DAS method aims to synthesize the total output of the array toward a certain direction. It is performed by applying certain delays and/or shifts to signals measured at all the array elements and summing all the delayed signals.[42] In our methods, we start from the frequency spectrum $V_m^\beta(\omega)$ of the mth FBG sensor and apply both phase delay $\Delta_m(\omega, \mathbf{x})$ and spatial phase shift $\varphi(\omega, \mathbf{x})$ to achieve a delayed and shifted version of the original spectrum, $Z_m(\omega, \mathbf{x})$, now in frequency–space representation

$$Z_m(\omega, \mathbf{x}) = V_m^\beta(\omega)e^{j[-\varphi(\omega, \mathbf{x}) - \Delta_m(\omega, \mathbf{x})]} \tag{6}$$

and

$$\Delta_m(\omega, \mathbf{x}) = k(\omega)\frac{\mathbf{x}}{|\mathbf{x}|} \cdot \mathbf{p}_m \quad \text{and} \quad \varphi(\omega, \mathbf{x}) = -k(\omega)|\mathbf{x}| \tag{7}$$

Here, $k(\omega)$ is the frequency–wavenumber dispersion relation of the propagating Lamb waves. It is known that Lamb waves naturally undergo a spatial phase shift $\varphi(\omega, \mathbf{x})$ as they travel (from the wave source to the array). Thus, $-\varphi(\omega, \mathbf{x})$ is manually applied as seen in equation (6) in order to compensate such a spatial phase shift, and $-\Delta_m(\omega, \mathbf{x})$ is the phase delay applied to the mth FBG sensor. Note that since $\varphi(\omega, \mathbf{x})$ and $\Delta_m(\omega, \mathbf{x})$ include the dispersion relation $k(\omega)$, the dispersion effect in Lamb wave propagation is therefore taken into consideration.[41]

Using the inverse Fourier transform, $Z_m(\omega, \mathbf{x})$ in frequency–space representation can be transformed to the time–space domain, as follows

$$z_m(t, \mathbf{x}) = \mathcal{F}^{-1}[Z_m(\omega, \mathbf{x})] = \frac{1}{2\pi}\int_{-\infty}^{\infty} Z_m(\omega, \mathbf{x})e^{j\omega t}d\omega \tag{8}$$

The result $z_m(t, \mathbf{x})$ is a time–space representation of Lamb wave at the mth FBG after applying phase delay and spatial phase shift. By summing up all $z_m(t, \mathbf{x})$ from the array as well as considering weighting factor w_m, the pixel value at the source location **x** can be acquired as follows

$$P(\mathbf{x}) = \left| \sum_{m=0}^{M-1} w_m^* z_m(t = 0, \mathbf{x}) \right|^2 \tag{9}$$

where w_m^* represents the complex conjugate of the weighting factor w_m.[41] Using equation (9), an image of the plate can therefore be generated with the location of the source yielding the maximum pixel value.

For simplicity, equation (9) can be rewritten in the matrix format, as follows

$$P(\mathbf{x}) = \mathbf{w}^H(\mathbf{x})\hat{\mathbf{R}}(\mathbf{x})\mathbf{w}(\mathbf{x}) \tag{10}$$

where "H" indicates the Hermitian transpose operation and $\mathbf{w}(\mathbf{x})$ is a vector composed of weighting factor w_m. $\hat{\mathbf{R}}(\mathbf{x})$ is a "steered pseudo-covariance matrix,"[27] resulting from $\hat{\mathbf{R}}(\mathbf{x}) = \mathbf{z}(\mathbf{x})\mathbf{z}^H(\mathbf{x})$, in which the vector $\mathbf{z}(\mathbf{x})$ is composed of $z_m(t = 0, \mathbf{x})$. For most of DAS imaging, the weighting vector $\mathbf{w}(\mathbf{x})$ is normally set to the unit vector **1** (i.e. no weighting).[3] The unit weighting vector is adopted for the DAS imaging presented in this article.

Adaptive MV method. For phased arrays, weighting factor plays an important role in enhancing the array imaging performance.[42] The weighting factors can be fixed values which are easy to implement and computationally simple. However, fixed-value weighting factors still generate lower resolutions and higher sidelobes, compared to adaptive weighing factors that adapt their values to the characteristics of the observations.[42] MV method is one of the most commonly used adaptive imaging methods adopted for Lamb wave–based damage detection[27] as well as medical ultrasound imaging.[43] In this method, the weighting factors are determined with the purpose to emphasize the pixel values in the direction of the wave source while to suppress the pixel values in other directions. That is to say, the weighting vector can be derived by solving the following constrained optimization problem

$$P(\mathbf{x}) = \arg\min_{\mathbf{w}} \mathbf{w}^H(\mathbf{x})\hat{\mathbf{R}}(\mathbf{x})\mathbf{w}(\mathbf{x})$$

such that

$$\mathbf{w}^H(\mathbf{x})\hat{\mathbf{e}}(\mathbf{x}) = 1 \qquad (11)$$

where $\hat{\mathbf{e}}(\mathbf{x})$ is a unit vector referred to as a "pseudo-steering vector." Since delaying for steering has already been implemented in equation (6), the "pseudo-steering vector" in equation (11) should take a simple formation not to disturb the steering, that is, as a unit vector 1. Therefore, the weighting vector of MV method becomes

$$\mathbf{w}_{MV}(\mathbf{x}) = \frac{\hat{\mathbf{R}}^{-1}(\mathbf{x})\mathbf{1}}{\mathbf{1}^T\hat{\mathbf{R}}^{-1}(\mathbf{x})\mathbf{1}} \qquad (12)$$

Accordingly, the pixel value at location $\mathbf{x}$ of the MV imaging becomes

$$P_{MV}(\mathbf{x}) = \mathbf{w}_{MV}^H(\mathbf{x})\hat{\mathbf{R}}(\mathbf{x})\mathbf{w}_{MV}(\mathbf{x}) \qquad (13)$$

Analytical imaging and characterization

Consider a linear FBG array with four sensors with uniform spacing $d = \lambda/2$ (a half wavelength). Analytical array imaging of three cases are studied:

1. Nonadaptive method using DAS without considering FBG sensor factor;
2. Nonadaptive method using DAS considering FBG's sensor factor $A(\beta) = \sin^2(\beta)$;
3. Adaptive method using MV considering FBG's sensor factor $A(\beta) = \sin^2(\beta)$.

Figure 4(a)–(c) gives the analytical imaging as pixel values for all directions for the three cases, when a wave source is at 90° direction (a.k.a. "broadside" of the array[3]). All cases show a mainlobe of the same magnitude with the center exactly at 90°. Comparing the results between cases (1) and (2) (Figure 4(a) and (b), respectively), it can be seen that the mainlobe has a smaller width and the sidelobes become reduced when FBG sensor factor is taken into consideration. Comparing the results between cases (2) and (3) (Figure 4(b) and (c), respectively), it can be seen that the mainlobe is significantly smaller and the sidelobes are highly suppressed with adaptive imaging. Hence, among the three cases via different imaging methods, the adaptive MV method generates the best imaging result for broadside detection (most focused mainlobe and lowest sidelobes) when the directional sensor factor has to be considered.

Figure 5(a)–(c) is the analytical imaging results when the wave source is at 45° direction (a.k.a. "offside" of
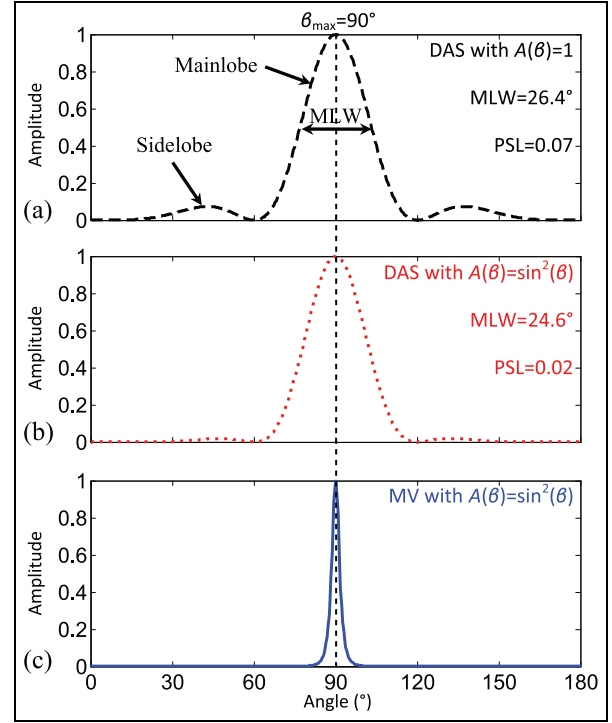
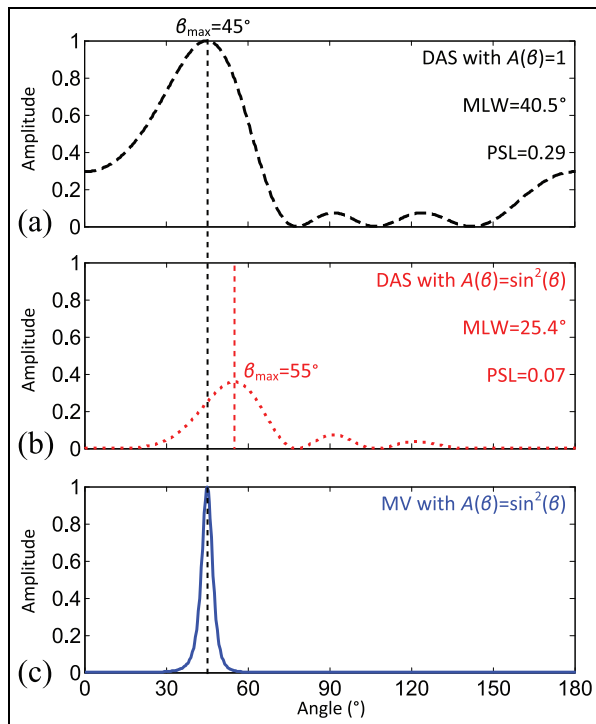

Figure 4. Analytical results when the wave source is at 90°: (a) DAS method with $A(\beta) = 1$, (b) DAS method with $A(\beta) = \sin^2(\beta)$, and (c) MV method with $A(\beta) = \sin^2(\beta)$. The MLW represents the width of the mainlobe at the half peak value. The PSL represents the peak value of the sidelobe.

the array[3]). Result of case (1) (Figure 5(a)) gives a correct indication of the wave source direction with its mainlobe centered at 45° but with large sidelobes resulted at various directions. Yet for case (2) (Figure 5(b)) when FBG sensor factor is considered, the mainlobe not only reduces in amplitude but also shifts to 55°, although some sidelobes are reduced. This indicates the DAS method is affected by the directional FBG sensing, and erroneous or distorted results with lower imaging quality will occur. With adaptive imaging used for case (3) (Figure 5(c)), however, we can see that the mainlobe is not only significantly focused at the target direction but also with a high amplitude, while the sidelobes are completely removed at the same time. Hence, among the three cases via different imaging methods, the adaptive MV method is the most reliable method with the best imaging quality for offside detection (most focused mainlobe and lowest sidelobes) when directional sensor factor has to be considered.

Damage detection with FBG phased arrays

Two sets of laboratory tests on plate specimens have been performed to detect simulated damage with the

Figure 5. Analytical results when the wave source is at 45°: (a) DAS method with $A(\beta) = 1$, (b) DAS method with $A(\beta) = \sin^2(\beta)$, and (c) MV method with $A(\beta) = \sin^2(\beta)$. The MLW represents the width of the mainlobe at the half peak value. The PSL represents the peak value of the sidelobe.

FBG Lamb wave phased arrays. The first test uses a linear array made of four FBG sensors to detect an actual wave source from a PZT actuator, while the second test uses the same FBG array to detect a surface damage simulated by a quartz rod bonded on the specimen.

Wave source detection

A schematic of experimental setup for detecting a wave source is given in Figure 6. The test specimen is a T3003 aluminum plate with dimensions of 610 mm × 610 mm × 1 mm. The plate center is defined as the coordinate origin O. The wave source is a PZT wafer that is bonded on the plate at a distance 150 mm to the Origin and angle β (90° or 45°) with respect to the x axis. The PZT excitation is three-count tone bursts at 270 kHz with an amplitude of 10 V, which will generate S_0 mode Lamb waves in the subject plate.[3] A four-FBG linear array is bonded on the plate with the array center at the Origin and spacing of 10 mm (a half of the S_0 mode wavelength at 270 kHz). In the array, the four FBGs on four separate fibers are identical (same length and reflection spectrum) so that they have the same response to the same mode of waves. For the purpose of phased array beamforming, the
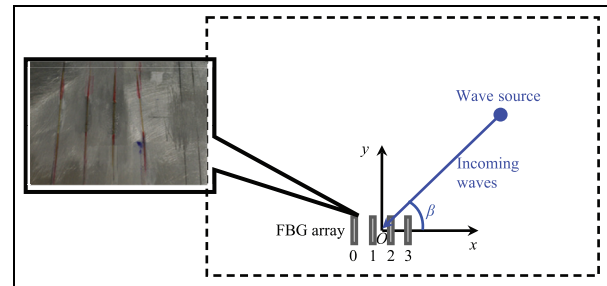
Figure 6. Experimental setup for detecting a wave source at β direction using a linear FBG array. The callout shows a close up photo of the FBG array.

signals of FBG sensors are not collected simultaneously, since our beamforming method is performed virtually as the post-signal processing. When Lamb waves are excited in the plate, FBG sensors will take turn to collect signals in a round-robin fashion. The collected signals are stored in a hard drive for the post-processing. Such switching from one FBG sensor to another is performed manually in the current test. Every time after the FBG is switched, we re-scan the reflection spectrum and lock the laser at the FWHM point.

Using the nonadaptive DAS and adaptive MV methods presented in section "FBG phased array imaging," images of the plate with the wave source at different β are generated, given in Figure 7 ($\beta = 90°$) and Figure 8 ($\beta = 45°$). The wave sources are presented as highlighted areas (large pixel values) in the intensity images. The results show that both methods successfully detect the wave sources at both directions 90° and 45°. Using the highest pixel value to estimate the source location, the detection errors of both methods for both directions are less than 5 mm.

Comparing the imaging results of the DAS and MV methods, it can be found that the adaptive MV method generates more focused images of the wave source than the DAS method, providing a better imaging resolution. Moreover, sidelobes are highly suppressed by the adaptive MV method, while the images generated by the nonadaptive DAS method show visible shadow rings in non-source directions. In addition, the MV method generates more focused images for waves coming in both broadside and offside directions, indicating it is less affected by the sensing direction β. Last, all the observations from the experimental results are consistent with the findings from the analytical results given in section "Analytical imaging and characterization."

Damage detection

Damage detection is performed by using the same FBG array to detect a surface bonded quartz rod (10 mm in
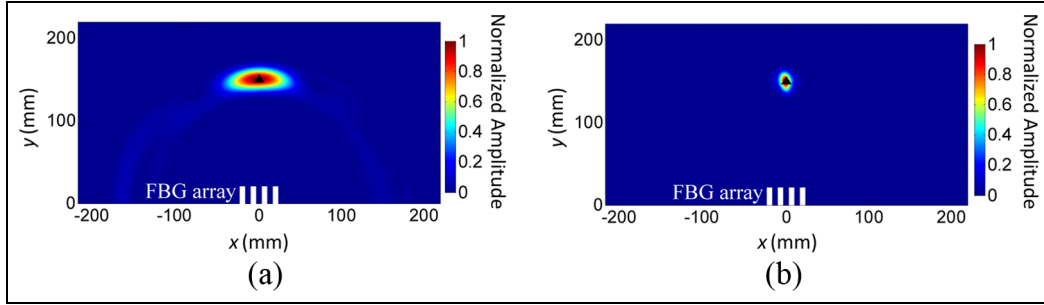
Figure 7. Array imaging results when the wave source is at $\beta = 90°$: (a) DAS method and (b) MV method. The black triangle represents the actual source location.
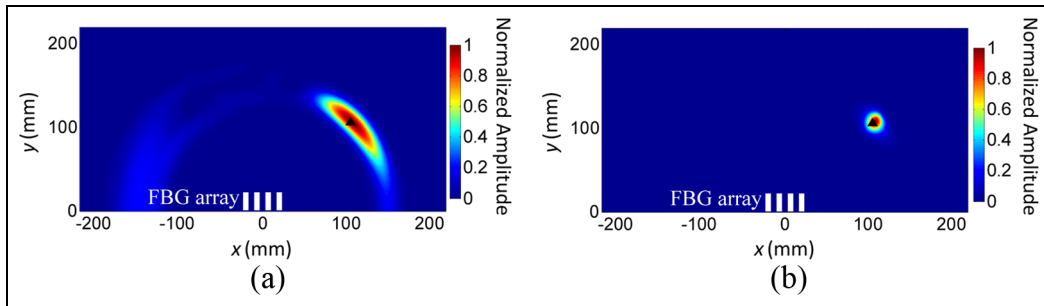
Figure 8. Array imaging results when the wave source is at $\beta = 45°$: (a) DAS method and (b) MV method. The black triangle represents the actual source location.

both diameter and height) at a distance 110 mm to the Origin and an angle β (90° or 45°) with respect to the x axis. Figure 9 shows the experimental setup. A PZT wafer is bonded at the location (30, 0) (unit: mm) to generate interrogation Lamb waves using three-count tone bursts at 270 kHz with the amplitude of 10 V as excitation signal. The generated S_0 Lamb wave will propagate in all directions, arrive at the simulated damage, and be reflected.

Considering the wave propagation from the source to the damage and then to the FBG array, the spatial phase shift in equation (7) now becomes

$$\varphi(\omega, \mathbf{x}) = -k(\omega)\left(|\mathbf{x}| + |\mathbf{x} - \mathbf{p}_{pzt}|\right) \qquad (14)$$

Equation (14) considers the total spatial phase shift in the entire propagation path and gives the general spatial phase shift for FBG array imaging.

Using the nonadaptive DAS and adaptive MV methods, images of the plate with damage at different β direction are generated, given in Figure 10 ($\beta = 90°$) and Figure 11 ($\beta = 45°$). The defects are presented as highlighted areas (large pixel values) in the intensity images. The results show that both methods successfully detect the presence of damage at both directions, 90° and 45°. Using the highest pixel value to estimate

the source location, the detection errors of both methods for both directions are less than 5 mm. Moreover, similar to the previous source detection case, the adaptive MV method generates more focused images of the damage with no sidelobe effect. Note for the damage detection at $\beta = 90°$ (Figure 10), the images of the damage look tilted for the reason that the PZT is not at the phase center of the FBG array, and the $\beta = 90°$ damage becomes offside to the PZT.
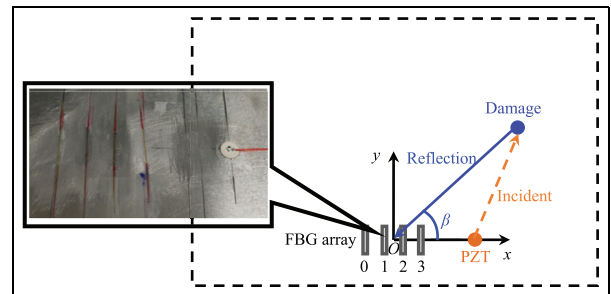

Figure 9. Experimental setup for detecting damage at β direction using a linear FBG array and a PZT actuator. The callout shows a close up photo of the FBG array and the PZT actuator.
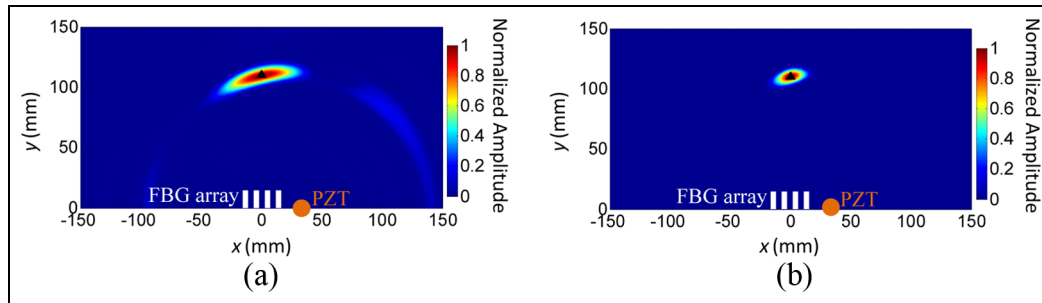
Figure 10. Array imaging results when the damage is at $\beta = 90°$: (a) DAS method and (b) MV method. The imaging results of both methods are tilted for the reason that the PZT is not at the phase center of the FBG array. The black triangle represents the actual damage location.
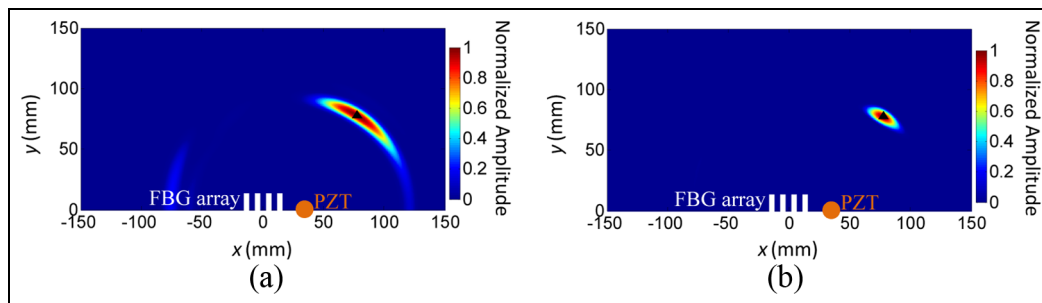
Figure 11. Array imaging results when the damage is at $\beta = 45°$: (a) DAS method and (b) MV method. The black triangle represents the actual damage location.

The received scattering waves at FBG are considered dominantly S_0 mode in this study. When an incident S_0 mode meets a simulated defect (a surface bonded rod here), the damage scattered waves could include both S_0 mode and additional weak A_0 mode resulted from mode conversion. Since the FBG sensors are relatively insensitive to the out-of-plane strain (dominated in the A_0 mode at the selected frequency) compared to the in-plane strain (dominated in the S_0 mode at the selected frequency),[16] the signals at them are mostly S_0 mode. This can also be verified by the damage imaging results. In our imaging method, the frequency–wavenumber relation (i.e. group velocity) of the S_0 mode is used, and the imaging result agrees well with the actual damage location with small errors less than 5 mm. This means that the received damage induced waves are mainly S_0 mode. If the actual signals were A_0 mode, the results would exhibit significant error since velocity of S_0 and A_0 is distinctively different (the group velocity of A_0 mode is much lower than that of the S_0 mode) in the subject material.[3]

Conclusion

In this study, we showed directional sensitivity FBG sensors that are arranged in a compact phased array

format can detect and localize wave sources and damage at various locations through adaptive phased array imaging. This innovative approach explicitly addresses the challenges raised by the directional sensitivity of FBG sensors and allows for robust localization of damage through adaptive imaging with enhanced resolution. It represents the first time that a compact configuration of FBG sensors for damage localization is achieved with the direction-dependent sensor factor being considered, to the best knowledge of the authors. Moreover, the FBG phased array offers inherent features such as immunity to electromagnetic interference, small, lightweight, embeddable, water-proof, and multiplexing, providing different features compared to existing phased arrays made of other types of transducers (PZT, EMAT, etc.).

To achieve this, we analytically studied the properties of two phased array imaging algorithms, the nonadaptive DAS and adaptive MV methods, and compared them in details. It is found that the adaptive MV method has a more focused mainlobe and highly suppressed sidelobes, generating localization images with better resolution and quality. In addition, the adaptive MV method well addresses the direction dependence of FBG Lamb wave sensing, offering localization images with high resolution and quality for all

directions. Results from experimental investigations are consistent, with errors less than 5 mm. It confirms that adaptive FBG phased array imaging provides a compact and robust methodology for damage localization in plate-like structures. In the framework of linear FBG phased arrays developed successfully in this article, further studies will be pursued to address multiple defects and extend to damage localization in composite structures.

Declaration of conflicting interests

Funding

References

1. Giurgiutiu V and Soutis C. Enhanced composites integrity through structural health monitoring. *Appl Compos Mater* 2012; 19: 813–829.
2. Staszewski WJ, Mahzan S and Traynor R. Health monitoring of aerospace composite structures—active and passive approach. *Compos Sci Technol* 2009; 69: 1678–1685.
3. Giurgiutiu V. *Structural health monitoring with piezoelectric wafer active sensors.* Boston, MA: Academic Press, 2008.
4. Rose JL. *Ultrasonic waves in solid media.* New York: Cambridge University Press, 1999.
5. Zhao XL, Qian T, Mei G, et al. Active health monitoring of an aircraft wing with an embedded piezoelectric sensor/actuator network: II. Wireless approaches. *Smart Mater Struct* 2007; 16: 1218–1225.
6. Michaels JE and Michaels TE. Guided wave signal processing and image fusion for in situ damage localization in plates. *Wave Motion* 2007; 44: 482–492.
7. Wilcox PD. Omni-directional guided wave transducer arrays for the rapid inspection of large areas of plate structures. *IEEE T Ultrason Ferr* 2003; 50: 699–709.
8. Su ZQ, Ye L and Lu Y. Guided Lamb waves for identification of damage in composite structures: a review. *J Sound Vib* 2006; 295: 753–780.
9. Perez I, Cui HL and Udd E. Acoustic emission detection using fiber Bragg gratings. *Proc SPIE* 2001; 4328: 209–215.
10. Betz DC, Thursby G, Culshaw B, et al. Acousto-ultrasonic sensing using fiber Bragg gratings. *Smart Mater Struct* 2003; 12: 122–128.
11. Peters K. Fiber Bragg grating sensors. In: Boller C, Chang FK and Fujino Y (eds) *Encyclopedia of structural health monitoring.* Hoboken, NJ: John Wiley & Sons, 2008, pp. 1097–1113.
12. Lam PM, Lau KT, Ling HY, et al. Acousto-ultrasonic sensing for delaminated GFRP composites using an embedded FBG sensor. *Opt Laser Eng* 2009; 47: 1049–1055.
13. Takeda N, Okabe Y, Kuwahara J, et al. Development of smart composite structures with small-diameter fiber Bragg grating sensors for damage detection: quantitative evaluation of delamination length in CFRP laminates using Lamb wave sensing. *Compos Sci Technol* 2005; 65: 2575–2587.
14. Kersey AD, Davis MA, Patrick HJ, et al. Fiber grating sensors. *J Lightwave Technol* 1997; 15: 1442–1463.
15. Othonos A. Fiber Bragg gratings. *Rev Sci Instrum* 1997; 68: 4309–4341.
16. Betz DC, Thursby G, Culshaw B, et al. Structural damage location with fiber Bragg grating rosettes and Lamb waves. *Struct Health Monit* 2007; 6: 299–308.
17. Tsuda H, Toyama N, Urabe K, et al. Impact damage detection in CFRP using fiber Bragg gratings. *Smart Mater Struct* 2004; 13: 719–724.
18. Wu ZJ, Qing XLP and Chang FK. Damage detection for composite laminate plates with a distributed hybrid PZT/FBG sensor network. *J Intel Mat Syst Str* 2009; 20: 1069–1077.
19. Kirkby E, De Oliveira R, Michaud V, et al. Impact localisation with FBG for a self-healing carbon fiber composite structure. *Compos Struct* 2011; 94: 8–14.
20. Betz DC, Staszewski WJ, Thursby G, et al. Structural damage identification using multifunctional Bragg grating sensors: II. Damage detection results and analysis. *Smart Materials & Structures* 2006; 15: 1313–1322.
21. Betz DC, Thursby G, Culshaw B, et al. Identification of structural damage using multifunctional Bragg grating sensors: I. Theory and implementation. *Smart Mater Struct* 2006; 15: 1305–1312.
22. Lin B and Giurgiutiu V. Development of optical equipment for ultrasonic guided wave structural health monitoring. In: *Proceedings of the SPIE 2014 smart structures and NDE*, San Diego, CA, 10 April 2014, p. 9062. Bellingham, WA: SPIE.
23. Minakuchi S, Okabe Y and Takeda N. Real-time detection of debonding between honeycomb core and facesheet using a small-diameter FBG sensor embedded in adhesive layer. *J Sandw Struct Mater* 2007; 9: 9–33.
24. Yu L and Giurgiutiu V. In situ 2-D piezoelectric wafer active sensors arrays for guided wave damage detection. *Ultrasonics* 2008; 48: 117–134.
25. Ambrozinski L, Stepinski T and Uhl T. Efficient tool for designing 2D phased arrays in Lamb waves imaging of isotropic structures. *J Intel Mat Syst Str* 2015; 26: 2283–2294.
26. De Marchi L, Moll J and Marzani A. A sparsity promoting algorithm for time of flight estimation in guided waves-based SHM. In: *Proceedings of the EWSHM-7th European workshop on structural health monitoring*, Nantes, 8–11 July 2014, pp. 583–590. French institute of science and technology for transport, spatial planning, development and networks (IFSTTAR).

27. Engholm M, Stepinski T and Olofsson T. Imaging and suppression of Lamb modes using adaptive beamforming. *Smart Mater Struct* 2011; 20: 850.

28. Giurgiutiu V and Bao J. Embedded-ultrasonics structural radar for in situ structural health monitoring of thin-wall structures. *Struct Health Monit* 2004; 3: 121–140.

29. Yoo B, Purekar AS, Zhang Y, et al. Piezoelectric-paint-based two-dimensional phased sensor arrays for structural health monitoring of thin panels. *Smart Mater Struct* 2010; 19: 750.

30. Fromme P, Wilcox PD, Lowe MJS, et al. On the development and testing of a guided ultrasonic wave array for structural integrity monitoring. *IEEE T Ultrason Ferr* 2006; 53: 777–785.

31. Kim D and Philen M. Guided wave beamsteering using MFC phased arrays for structural health monitoring: analysis and experiment. *J Intel Mat Syst Str* 2010; 21: 1011–1024.

32. Malinowski P, Wandowski T, Trendafilova I, et al. A phased array-based method for damage detection and localization in thin plates. *Struct Health Monit* 2009; 8: 5–15.

33. Ostachowicz W, Kudela P, Malinowski P, et al. Damage localisation in plate-like structures based on PZT sensors. *Mech Syst Signal Pr* 2009; 23: 1805–1829.

34. Purekar AS, Pines DJ, Sundararaman S, et al. Directional piezoelectric phased array filters for detecting damage in isotropic plates. *Smart Mater Struct* 2004; 13: 838–850.

35. Rajagopalan J, Balasubramaniam K and Krishnamurthy CV. A single transmitter multi-receiver (STMR) PZT array for guided ultrasonic wave based structural health monitoring of large isotropic plate structures. *Smart Mater Struct* 2006; 15: 1190–1196.

36. Swift CI, Pierce SG and Culshaw B. Generation of a steerable ultrasonic beam using a phased array of low power semiconductor laser sources and fiber optic delivery. *Smart Mater Struct* 2007; 16: 728–732.

37. Velichko A and Wilcox PD. Guided wave arrays for high resolution inspection. *J Acoust Soc Am* 2008; 123: 186–196.

38. Deutsch WAK, Cheng A and Achenbach JD. Self-focusing of Rayleigh waves and Lamb waves with a linear phased array. *Res Nondestruct Eval* 1997; 9: 81–95.

39. Purekar AS and Pines DJ. Damage detection in thin composite laminates using piezoelectric phased sensor arrays and guided Lamb wave interrogation. *J Intel Mat Syst Str* 2010; 21: 995–1010.

40. Leleux A, Micheau P and Castaings M. Long range detection of defects in composite plates using Lamb waves generated and detected by ultrasonic phased array probes. *J Nondestruct Eval* 2013; 32: 200–214.

41. Yu LY and Tian ZH. Guided wave phased array beamforming and imaging in composite plates. *Ultrasonics* 2016; 68: 43–53.

42. Johnson DH and Dudgeon DE. *Array signal processing: concepts and techniques.* Upper Saddle River, NJ: Prentice-Hall Inc., 1993.

43. Synnevag JF, Austeng A and Holm S. Adaptive beamforming applied to medical ultrasound imaging. *IEEE T Ultrason Ferr* 2007 54: 1606–1613.